



Here  $E_{em} = \frac{e^2 E^2}{4m}$  is the energy induced by the RF due to the DFKE,<sup>12,13</sup>  $E_{em} = 2$ ;  $f(r)g$  can be any set of complete basis.  $fF_n g$  are the eigenvectors of the equations:<sup>29</sup>

$$\sum_{m=1}^N h_{nj_F j m i} F_m = \epsilon F_n; \quad (3)$$

in which  $h_{nj_F j m i} = \langle r | e^{i n t} H_F = H(t) | i \rangle_t$  and  $h_{nj_F j m i} = H^{n m} + m \sum_{nm} w_{nm}$  with  $H^n = \frac{1}{T_0} \int_0^{T_0} dt e^{i n t} H(t)$  representing the  $n$ -th Fourier component of the Hamiltonian. The eigen-values  $\epsilon$  of the equations are solved in the region  $(\epsilon = 2; \epsilon = 2)$ .<sup>29</sup> In the case of the Rashba SOC, the non-zero terms are

$$H^0 = \frac{p^2}{2m} + \frac{1}{2} m \omega_0^2 r^2 + \alpha_R [\hat{x} p_y - \hat{y} p_x]; \quad (4)$$

$$H^1 = (H^{-1})^\dagger = \frac{i e E}{2m} p_x - \frac{i \alpha_R e E}{2} \hat{y}; \quad (5)$$

with  $p = -i \nabla$ .

We choose the complete basis  $f g$  to be the eigenstates of the single spin in a QD without the RF and the SOC, whose Hamiltonian is described by the first two terms of Eq. (4). These states are identified as  $f|N; l\rangle_i$  with

$$\langle r | N; l; i \rangle = \frac{N!}{a^2 (N-l)!} \frac{r^l}{(N-l)!} L_{N-l}^{lj}((r/a)^2) e^{i l \phi} \quad (6)$$

Here  $r = (r \cos \phi; r \sin \phi)$ ;  $a = \sqrt{\frac{2}{m \omega_0}}$ ;  $L_{N-l}^{lj}$  is the Laguerre polynomial;  $n_r = (N-l)-2$ ; and  $i$  is the eigenspinor of  $\sigma_z$ . With these basis functions one is able to write out the matrix  $H_F$  and numerically diagonalize it.<sup>30</sup> In this way, one obtains the eigenvalues  $\epsilon$  and the eigenvectors  $fF_n g$ .

Without the RF and the SOC, the eigenstates of a single spin in the QD  $|N; l; i\rangle$  are  $2(N+1)$ -fold degenerate in angular momentum (index  $l = N; N+2; \dots; N-2; N$ ) and spin momentum (index  $i = \uparrow, \downarrow$ ), with energy being  $(N+1)\epsilon_0$ . The degeneracy is partially lifted by the

SOC into  $(N+1)$  states, each with 2-fold Kramers degeneracy. Although these states are no longer eigenstates of  $\sigma_z$ , they can be distinguished by the corresponding majority spin components as quasi-spin-up and -down states.<sup>10,30</sup> The schematic of the lowest 12 states together with the possible transitions among them is shown in Fig. 1. For both the small SOC and the small RF, the transitions are mainly between the states in the same quasi-spin branch (the solid arrows in Fig. 1), since the RF does not flip the spin. At high RF and/or high SOC, the direct transitions (the dotted arrows) and multiphoton processes between different quasi-spin branches are important, therefore the two quasi-spin branches become strongly mixed. The mixing can be roughly quantified by the quantity  $\alpha = \alpha_R e E / (\hbar \omega)$  which comes from the photon-assisted spin flip (the second term of  $H^1$ ) divided by the THz frequency.<sup>22</sup> The stronger the correlation between different spin branches is, the larger  $\alpha$  becomes.

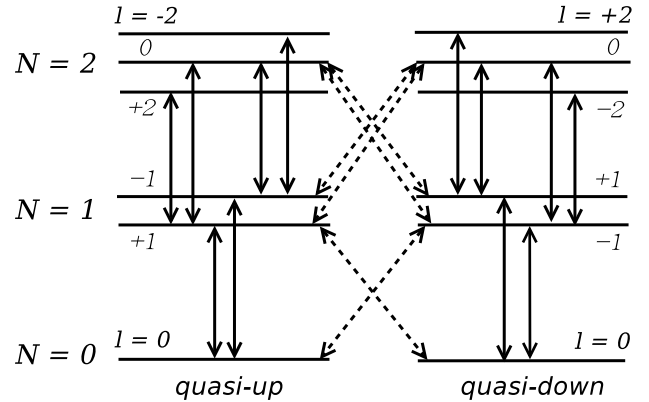


FIG. 1: Schematic of the lowest 12 states of zero field Hamiltonian  $H^0$ , with all possible transitions. The transitions are indicated by solid arrows for quasi-spin conserving transitions and dotted arrows for quasi-spin flip transitions.

The effects of the RF and SOC can be qualified by the density of states (DOS),  $\rho$ , and density of spin polarization (DOSP),  $\rho_s$ .<sup>22</sup> These densities can be calculated from spectral functions which can be extracted from the Green functions:

$$\begin{aligned} G_{1,2}^{\pm}(\mathbf{r}; \epsilon) &= \frac{1}{2\pi i} \int_{-\infty}^{\infty} dt e^{i\epsilon t} \int d^2 r G_{1,2}^{\pm}(\mathbf{r}; t_1; t_2) G_{1,2}^{\pm}(\mathbf{r}; t_1; t_2) \\ &= \frac{1}{2\pi i} \int_{-\infty}^{\infty} dt e^{i\epsilon t} \int d^2 r G_{1,2}^{\pm}(\mathbf{r}; t_1) G_{1,2}^{\pm}(\mathbf{r}; t_2) \\ &= \sum_{p, m, n} g_{1,2}(\mathbf{r}; \epsilon; \mathbf{r}) F_n F_m J_p(2 \cos(2 T)) \exp[i(n-m) T] \\ & \quad (| \epsilon | - | \epsilon' + E_{em} | (2p + n + m) = 2); \end{aligned} \quad (7)$$

where  $G^r$  and  $G^a$  are retarded and advanced Green's functions respectively,  $T = (t_1 + t_2)/2$ ,  $t = t_1 - t_2$ , and stand for  $f_N$ ;  $g$ ,  $J_p$  is the Bessel function of  $p$ -th order and

$$\begin{aligned} g_{1/2} &= f_N; g = f_N^{0,1,0}; g \\ &= h^{-1} j_2 i = N; N^{0,1,0}; 2; 0: \end{aligned} \quad (8)$$

It is seen from Eq. (7) that these densities are periodic functions of  $T$  with period  $T_0$ . Symmetry analysis (time reversal symmetry and parity symmetry) further suggests that there is no spin polarization along the  $x$ - and  $z$ -axis. The only non-vanishing component of the spin polarization is along the  $y$ -axis and reduces to zero if the RF is turned off. The spin polarization is an odd function of time;  $\langle T; \rangle = -\langle T; \rangle$ , and therefore there is no overall spin polarization once averaged over time. On the other hand, the DOS is an even function of time and  $\langle T; \rangle = \langle T; \rangle$ . Thus the RF and the SOC can affect the overall DOS, but cannot induce any spin polarization along the  $z$ -axis. In order to account for the effect of the RF and the SOC on the system, we use the average of  $\langle T; \rangle$  over a period to quantify the DOS

$$\langle \rho \rangle = \frac{1}{T_0} \int_0^{T_0} \rho(T) dT; \quad (9)$$

By numerically diagonalizing the matrix  $H_F$ , one is able to obtain the coefficients  $f_n$  and then calculate the DOS and the DOSP through Eq. (7). One can further obtain the time-averaged DOS by using Eq. (9) and calculate the magnetic moment along the  $y$ -axis  $M_y$  via proper evaluation of  $\hbar y_i$ .<sup>22</sup> To converge the DOS in the energy range between 0 to  $2.4\epsilon_0$ , one has to use as many as 132 states from the lowest 11 major shells ( $N = 0-10$ ) since the energy levels of the QD are almost equidistant and hence lead to significant resonant overlap.<sup>29</sup> In the following we present the numerical results of the time-averaged DOS and the magnetic moment  $M_y$  under different conditions. In the calculation, the effective mass  $m = 0.023m_0$  with  $m_0$  representing the free electron mass and the Rashba coefficient  $R = 3 \times 10^9$  eV cm.<sup>27,28</sup> The confinement potential  $\epsilon_0$  is chosen to be 5 THz, which corresponds to a QD with diameter about 55 nm.<sup>4,30,31</sup>

In Fig. 2 we compare the time-averaged DOS with and without the SOC or the RF. The red (solid) curves are the DOS with both the SOC and the RF when  $E = 0.6$  kV/cm and  $\omega = 4$  THz. The blue (dotted) curve in Fig. 2(a) is the DOS with only the SOC while the one in (b) is the DOS with only the RF. It is noted that in the figure the  $\rho$ -function  $\rho(x)$  in the DOS is replaced by the Gaussian function  $\exp(-x^2/2) = (\frac{1}{\sqrt{2\pi}}) \exp(-x^2/2)$  with  $\sigma = 0.005\epsilon_0$ . The DOS without the SOC and the RF peaks at  $\epsilon = (N+1)\epsilon_0$  with value  $(N+1) = (\frac{1}{2})(N+1)$  ( $N = 0; 1; 2$ ; with the lowest two levels labelled by dashed lines in the figure). Each level has  $(N+1)$ -fold degeneracy as pointed out above. Nevertheless, by including only the SOC, the 2-fold degeneracy of  $N = 1$  major shell is lifted and the

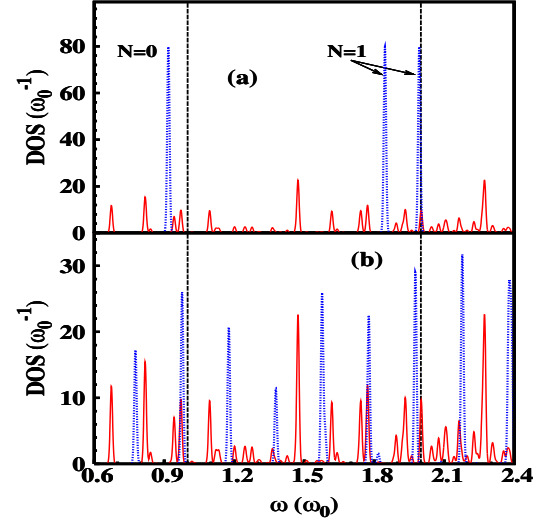


FIG. 2: (Color online) (a) The time-averaged DOS of QD under THz field with  $E = 0.6$  kV/cm,  $\omega = 4$  THz (red solid curve) and  $E = 0$  (blue dotted curve) for  $R = 3 \times 10^9$  eV cm. (b) The time-averaged DOS of QD with Rashba SOC  $R = 3 \times 10^9$  eV cm (red solid curve) and  $R = 0$  (blue dotted curve) for  $E = 0.6$  kV/cm,  $\omega = 4$  THz. The black dashed lines correspond to the positions of  $\epsilon_0$  and  $2\epsilon_0$ .

ground state energy ( $N = 0$ ) is lowered by  $0.1\epsilon_0$ , as indicated in Fig. 2(a). Moreover, including only the RF gives rise to many peaks at the integer multiplications of  $\epsilon_0$ , as can be seen in Eq. (7). It is seen from Fig. 2(b) that these peaks are equidistant. The peaks are generally higher than those in the case with both the RF and the SOC, as the SOC causes additional splitting of the degenerate states.

In order to further reveal the effect of the SOC and the RF on the system, we study the DOS under different RF and SOC. In Fig. 3, the DOS with different RF strengths (a) and Rashba coefficients (b) are plotted against energy. It is seen from Fig. 3(a) that the first peak of the DOS gets a red shift from  $0.75\epsilon_0$  when  $E = 0.5$  kV/cm to  $0.68\epsilon_0$  when  $E = 0.6$  kV/cm and then comes back to  $0.74\epsilon_0$  when  $E$  is further increased to  $0.7$  kV/cm. This is a clear demonstration of the combined effect of the AC Stark effect and the DFKE.<sup>14</sup> The AC Stark effect, which states that the energy difference becomes larger (smaller) if two energy levels are driven by an AC field with frequency below (above) the resonance.<sup>14,15</sup> On the other hand, the DFKE states that the DOS has a blue-shift due to  $E_{em}$  as indicated in Eq. (7).<sup>12,13</sup> In the current case, the frequency of the THz irradiation is 4 THz, which is smaller than the resonant frequencies of the transitions from  $N = 0$  to  $N = 1$  major shells even when the SOC is included. Therefore there is an AC Stark effect which shifts the  $N = 0$  major shell to red-side. This effect is responsible for the red shifts as the DOS in the low energy range mainly consists of  $N = 0$  major shell. Although both the DFKE blue-shift  $E_{em}$  and the AC

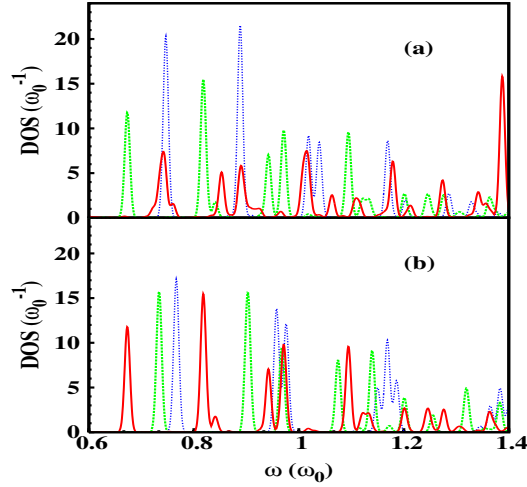


FIG. 3: (Color online) The time-averaged DOS (a) for  $E = 0.5$  (green dot-dashed curve),  $0.6$  (blue dotted curve) and  $0.7$  (red solid curve) kV/cm, with  $E_R = 3 \times 10^9$  eV/cm and  $\omega = 4$  THz and (b) for  $E_R = 1$  (green dot-dashed curve),  $2$  (blue dotted curve) and  $3$  (red solid curve)  $10^9$  eV/cm, with  $E = 0.6$  kV/cm and  $\omega = 4$  THz.

Stark red-shift increase with the RF strength, the AC Stark effect is more important at low RF strength, and it saturates at high RF strength where the blue-shift due to the DFKE dominates.<sup>14</sup> Moreover, at low RF intensity the peaks locate at  $\omega = \omega_0 \pm E_{em}$  of a certain  $n_0$  or replicas  $\omega = \omega_0 \pm E_{em}(n_0 + n)$  with small  $n$ 's. When the RF increases, the multi-photon processes become more and more important. As a result, the DOS becomes smoother as more and more multi-photon replicas appear. The effect of the SOC is plotted in Fig. 3(b), where the DOS under different Rashba coefficient  $E_R$  is plotted when the RF  $E = 0.6$  kV/cm and  $\omega = 4$  THz. It is seen that the first peak shifts to the red side as  $E_R$  increases. This is understood as the SOC contributes to the AC Stark effect. From Eq. (5), one notices that the AC Stark effect enhances as the SOC is increased. Differing from the situation shown in Fig. 3(a), the blue shift  $E_{em}$  from the DFKE does not change since the RF is fixed here. Therefore the shift of the first DOS peak is monotonic. Moreover, as  $E_R$  increases the multi-photon processes between different spin branches become more important and the DOS becomes smoother.

As said before, the DOS is not zero when both the SOC and the RF are present. Due to the symmetry of the system, the only remaining spin polarization is along the y-axis. Consequently, the induced average magnetic moment can be calculated through the equation<sup>22</sup>

$$M_y(T) = \frac{1}{Z} \sum_{\mathbf{n}} \langle \mathbf{n} | \hat{M}_y | \mathbf{n} \rangle e^{-\beta E_{\mathbf{n}}(T)} / \sum_{\mathbf{n}} e^{-\beta E_{\mathbf{n}}(T)}; \quad (10)$$

where the time-dependent Fermi energy  $E_F(T)$  is determined by  $2 \sum_{\mathbf{n}} e^{-\beta E_{\mathbf{n}}(T)} = 1$  when there is only one electron in the quantum dot. Due to the time periodicity introduced by the THz field,  $E_F(T)$  and  $M_y(T)$  are also periodic functions of  $T$  with period  $T_0$ . In Fig. 4, we plot the y-component of magnetic moment as a function of time. The magnetic moment is controlled by the RF strength, the frequency as well as the SOC and it can be qualitatively described by the factor  $E_R$ . The stronger the RF and the SOC are, the larger  $M_y$  becomes. On the other hand, the larger  $\omega$  is, the smaller  $M_y$  becomes and therefore the smaller  $M_y$  becomes.

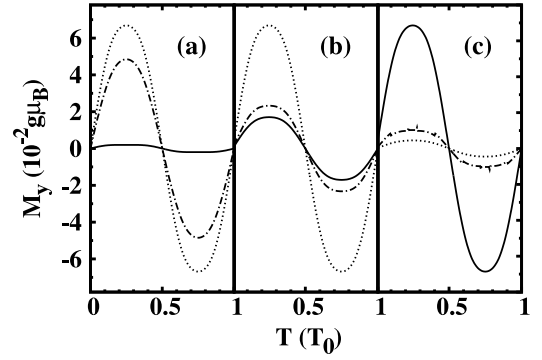


FIG. 4: The average magnetic moment  $M_y$  versus the time for a single spin in QD at (a)  $E = 0.3$  (solid curve),  $0.5$  (dotted curve), and  $0.6$  (dot-dashed curve) kV/cm for fixed  $\omega = 4$  THz, and  $E_R = 3 \times 10^9$  eV/cm; (b)  $E_R = 1$  (solid curve),  $1.5$  (dotted curve), and  $3$  (dot-dashed curve)  $10^9$  eV/cm for fixed RF with  $\omega = 4$  THz and  $E = 0.6$  kV/cm; (c)  $E = 0.6$  kV/cm,  $\omega = 4$  THz, and  $E_R = 4$  (solid curve),  $4.6$  (dotted curve), and  $6$  (dot-dashed curve)  $10^9$  eV/cm.

In conclusion, we study the effects of the intense THz field on single electron spin in QD with the Rashba SOC. We calculate the single electron DOS at zero temperature and show that the DOS is greatly affected by the THz field and the SOC due to the dynamic Franz-Keldysh effect, the AC Stark effect and the side-band effect. It is shown that the joint effect of the THz field and the SOC can excite a THz magnetic moment which is controlled by the THz field strength, the THz frequency as well as the SOC. This provides a unique way to convert THz electric signals into THz magnetic ones which may be useful in full electrical magnetic resonance measurements.

This work was supported by the Natural Science Foundation of China under Grant Nos. 90303012 and 10574120, the Natural Science Foundation of Anhui Province under Grant No. 050460203, the Knowledge Innovation Project of Chinese Academy of Sciences and SRFDP. J.H.J. would like to thank J.L.Cheng for helpful discussions.

- 
- <sup>1</sup> D. Loss and D. P. DiVincenzo, Phys. Rev. A 57, 120 (1998).
  - <sup>2</sup> V. Cerletti, W. A. Coish, O. Gywat, and D. Loss, Nanotechnology 16, R27 (2005), and references there in.
  - <sup>3</sup> H. A. Engel, L. P. Kouwenhoven, D. Loss, and C. M. Marcus, Quantum Information Processing 3, 115 (2004), and reference there in.
  - <sup>4</sup> V. N. Golovach, A. Khaetskii, and D. Loss, Phys. Rev. Lett. 93, 016601 (2004).
  - <sup>5</sup> Semiconductor spintronics and quantum computation, ed. by D. D. Awschalom, D. Loss, and N. Samarth (Springer, Berlin, 2002).
  - <sup>6</sup> I. Zutic, J. Fabian, and S. Das Sarma, Rev. Mod. Phys. 76, 323 (2004).
  - <sup>7</sup> Y. Y. Wang and M. W. Wu, cond-mat/0601028.
  - <sup>8</sup> J. M. Elzerman, R. Hanson, L. H. Willems van Beveren, B. Witkamp, L. M. K. Vandersypen, and L. P. Kouwenhoven, Nature 430, 431 (2004).
  - <sup>9</sup> A. S. Bracker, E. A. Stinaff, D. Gammon, M. E. Ware, J. G. Tischler, A. Shabaev, A. L. Efros, D. Park, D. Gershoni, V. L. Korenev, and I. A. Merkulov, Phys. Rev. Lett. 94, 047402 (2005).
  - <sup>10</sup> M. Valin-Rodriguez, A. Puente, and L. Serra, Phys. Rev. B 66, 045317 (2002).
  - <sup>11</sup> Y. Yacoby, Phys. Rev. 169, 610 (1968).
  - <sup>12</sup> A. P. Jauho and K. Johnsen, Phys. Rev. Lett. 76, 4576 (1996).
  - <sup>13</sup> K. Johnsen and A. P. Jauho, Phys. Rev. B 57, 8860 (1998).
  - <sup>14</sup> K. B. Nordstrom, K. Johnsen, S. J. Allen, A. P. Jauho, B. Bimir, J. Kono, and T. Noda, Phys. Rev. Lett. 81, 457 (1998).
  - <sup>15</sup> A. H. Rodriguez, L. M. ezamontes, C. Trallero-Giner, and S. E. Ulloa, phys. stat. sol. (b) 242, 1820 (2005).
  - <sup>16</sup> J. Ceme, K. Kono, T. Inoshita, M. Sundaram, and A. C. Gossard, Appl. Phys. Lett. 70, 3543 (1997).
  - <sup>17</sup> J. Kono, M. Y. Su, T. Inoshita, T. Noda, M. S. Sherwin, S. J. Allen, Jr., and H. Sakaki, Phys. Rev. Lett. 79, 1758 (1997).
  - <sup>18</sup> C. Phillips, M. Y. Su, M. S. Sherwin, J. Ko, and L. Coldren, Appl. Phys. Lett. 75, 2728 (1999).
  - <sup>19</sup> M. G. Riffoni and P. Hanggi, Phys. Rep. 304, 229, and reference there in.
  - <sup>20</sup> S. Kohler, J. Lehmann, and P. Hanggi, Phys. Rep. 406, 379, and reference there in.
  - <sup>21</sup> L. Arrachea, Phys. Rev. B 72, 125349 (2005), and reference there in.
  - <sup>22</sup> J. L. Cheng and M. W. Wu, Appl. Phys. Lett. 86, 032107 (2005).
  - <sup>23</sup> C. M. Wang, S. Y. Liu, and X. L. Lei, Phys. Rev. B 73, 035333 (2006).
  - <sup>24</sup> Y. A. Bychkov and E. Rashba, Sov. Phys. JETP Lett. 39, 78 (1984).
  - <sup>25</sup> R. Winkler, Spin-Orbit Coupling Effects in Two-Dimensional Electron and Hole Systems (Springer, Berlin, 2003).
  - <sup>26</sup> G. Dresselhaus, Phys. Rev. 100, 580 (1955).
  - <sup>27</sup> D. Grundler, Phys. Rev. Lett. 26, 6074 (2000).
  - <sup>28</sup> Y. Sato, T. Kita, S. Gozu, and S. Yamada, J. Appl. Phys. 89, 8017 (2001).
  - <sup>29</sup> J. H. Shirley, Phys. Rev. 138, B979 (1965).
  - <sup>30</sup> J. L. Cheng, M. W. Wu, and C. Lu, Phys. Rev. B 69, 115318 (2004).
  - <sup>31</sup> R. Hanson, B. Witkamp, L. M. K. Vandersypen, L. H. Willems van Beveren, J. M. Elzerman, and L. P. Kouwenhoven, Phys. Rev. Lett. 91, 196802 (2003).